CIMAC CONGRESS 25
ZURICH, MAY 19 – 23, 2025

2025 | 465

Exhaust aftertreatment concepts for two-stroke NH3 engines

Exhaust Gas Aftertreatment Solutions & CCS

Georgia Voniati , Laboratory of Applied Thermodynamics, Aristotle University of Thessaloniki

Athanasios Dimaratos, Laboratory of Applied Thermodynamics, Aristotle Univeristy of Thessaloniki
Grigorios Koltsakis, Laboratory of Applied Thermodynamics, Aristotle Univeristy of Thessaloniki
Leonidas Ntziachristos, Laboratory of Applied Thermodynamics, Aristotle Univeristy of Thessaloniki
Anker Jensen, Technical University of Denmark-DTU
Rishav Chand, Technical University of Denmark-DTU
Billie Lynn Abrams, Topsoe
Janus Emil Münster-Swendsen, Topsoe
Johan Sjöholm, MAN Energy Solutions
Hanne Falsig, Topsoe

DOI: https://doi.org/10.5281/zenodo.15229780

ABSTRACT

This paper summarizes the research activities conducted within the EU-funded H2020 “ENGIMMONIA” project aiming to develop low greenhouse gas marine transportation with ammonia fueled engines. In particular, this work presents the concept development of exhaust aftertreatment systems (EATS) aimed at reducing N-species (NOx, NH3, N2O) for emissions compliance and greenhouse gas minimization.

A focal point of the project is the elimination of N2O via combustion optimization, advanced catalytic coatings and careful adaptation of the exhaust system concept to address dual-fuel requirements (Diesel only or NH3 with pilot Diesel). Since combustion optimization is a slow process, the exhaust gas composition and temperature are not fixed to allow for the EATS design on time. Therefore, a flexible, model-supported approach is followed to prepare the emission control for a variety of possible engine-out emissions scenarios.

The research for catalytic exhaust after-treatment included both traditional materials as well as innovative ones to deal with N2O, if necessary. Promising catalyst materials targeting N2O are synthesized, screening for activity in powder form in a plug flow reactor. Iron-based SCR (Fe-SCR) and technology is utilized into a monolith which is then tested on a Synthetic Gas Bench (SGB), replicating the exhaust gas conditions of NH3 combustion. In addition, a typical commercial catalytic monolith sample for NH3 abatement (i.e., Ammonia Slip Catalyst (ASC)) is tested. The reaction kinetics derived from the gas bench are subsequently incorporated into physico-chemical models using the ExothermiaSuite® simulation platform. After a step-by-step improvement of the reaction scheme, the predictive capacity of the models is established in the entire operating envelope of the ammonia engine exhaust.

The model-based analysis proved that a promising configuration is based on engine calibration for low N2O and NH3 and rather high NOx emissions. This allows the use of SCR chemistry with additional NH3 injection in the exhaust for the abatement of NOx. An Fe-containing catalyst was found to be effective for deNOx and showed appreciable reduction of N2O at certain temperatures with NH3 presence. The tolerance to sulfur and its thermal removal were found to be compatible with the target dual-fuel engine application. The full-scale system is conceptualized, and a parametric optimization is presented that accounts for meeting the legislative Tier III NOx emissions requirements, while maintaining a greenhouse gas emissions benefit compared to a Diesel fueled engine.

1 INTRODUCTION

The maritime sector is responsible for nearly 3% of global greenhouse gas (GHG) emissions, a figure projected to rise by 2050 [1]. In addition to GHG emissions, maritime activities produce air pollutants, including nitrogen oxides (NO_x) [2]. To address the environmental challenges posed by shipping, the International Maritime Organization (IMO) has introduced stricter emission regulations, targeting a reduction of at least 70% in GHG emissions by 2040, with the ultimate goal of achieving net-zero GHG emissions by around 2050 [3]. Simultaneously, NO_x emissions must meet the Tier III standards (3.4g/kWh for low-speed two-stroke engines) withing Emission Control Areas (ECAs) and Tier II standards (14.4g/kWh for low-speed two-stroke engines) globally.

To achieve the GHG emission reduction goals, LNG and LPG serve as transitional fuels, offering lower emissions compared to conventional fossil fuels. Meanwhile, alternative fuels such as ammonia (NH_3), methanol (CH_3OH) and hydrogen (H_2) offer significant potential for long-term decarbonization. Among these, NH_3 stands out as a promising carbon-free option. However, its poor combustion properties require the use of a pilot fuel like diesel to initiate combustion [4,5]. Additionally, apart from unburnt NH_3 and NO_x, NH_3 combustion generates nitrous oxides (N_2O), a potent GHG with Global Warming Potential (GWP) nearly 300 times higher than that of CO_2 [6]. To fully mitigate the unwanted N-species, the Exhaust Aftertreatment System (EATS) in ammonia-fueled engines must be adopted accordingly. This paper summarizes the emissions relevant research activities conducted within the EU-funded H2020 “ENGIMMONIA” project aiming to develop low greenhouse gas marine transportation with ammonia fueled 2-stroke engines.

The main challenge is the simultaneous minimization of NO_x, NH_3 and N_2O through combustion optimization, advanced catalytic coatings, and exhaust system adaptation for dual-fuel operation (NH_3 with pilot Diesel). Combustion parameters can be tuned to balance NO_x, NH_3 and N_2O emissions. On the other hand, the exhaust after-treatment system design and controls can be designed for optimum performance depending on the exhaust gas conditions. This means that the final goal of emissions minimization relies on an optimum combination of engine combustion and EATS. This can be achieved via an iterative optimization process which is obviously too complex and time consuming unless it takes place in a simulation framework which is supported by predictive and validated mathematical models.

Compared to a traditional Diesel engine application, the optimization task involves additional challenges that are specific to the NH_3 combustion: (a) the EATS has to be designed to perform well under both 100% Diesel and NH_3 with pilot Diesel operation, (b) the EATS architecture is defined by the engine-out NH_3/NO_x (ANR) ratio. ANR lower than 1 would necessitate an additional reductant injection system whereas ANR>1 would necessitate NH_3 treatment. However, engine-out ANR is not fixed beforehand and may actually be an optimization parameter to the extent possible by the combustion parameters (c) As mentioned before, N_2O may come in non-negligible quantities from the combustion process and its reactivity in the catalytic system has to be investigated. The EATS related models rely on reaction kinetics rate equations derived from lab testing data. The N_2O problematic has led us to explore a variety of catalytic materials that could be potential candidates for N_2O catalytic decomposition.

Promising technologies, such as iron (Fe)-based SCR and cobalt (Co)-based catalyst are synthesized using methods like wet impregnation, ion exchange and co-precipitation. Such catalysts are screened for activity in powder form using a plug flow reactor. The Fe-BEA catalyst is applied onto a monolithic support which is then tested on a Synthetic Gas Bench (SGB) replicating the exhaust gas conditions of NH_3 combustion. The preparation of the monolith of the Co-based catalyst as well as testing and analysis are currently on-going. Hence, this study focuses on the application of the Fe-BEA. In addition, a commercial platinum-based ammonia oxidation catalyst (Pt-AOC) monolith is tested for the potential reduction of unreacted NH_3. The reaction kinetics derived from the gas bench are subsequently incorporated into physico-chemical models following calibration of the kinetics rate parameters. The validated exhaust system model is then applied at conditions relevant to the full-scale dual-fuel engine exhaust. In this way, it is possible to run a large number of parametric cases and study the impact of engine-out emissions, catalyst sizing and, where applicable, NH_3 dosing controls to achieve the project targets.

2 EXPERIMENTAL AND MODELING METHODS

2.1 Powder testing

2.1.1 Experimental setup and reaction parameters

Catalyst experiments were carried out at DTU in a quartz U-tube reactor (OD: 6mm, ID: 4mm) in the range of 150-500°C. 250 mL/min of gas mixture comprising of 250 ppm N2O, 250 ppm NH_3 (if used), 5% O_2, ~2.5% H_2O (if used) and balance N_2 was passed through a bed of 50 mg of catalyst

Figure 1. Reactor setup for testing the powder catalysts. The numbered sections in the figure refer to: 1) mass flow controllers for the feed gases, 2) bubbling set up (evaporator) for introducing H_2O in the feed, 3) heat-traced and insulated tubes for gas flow, and 4) furnace with the reactor contained within.

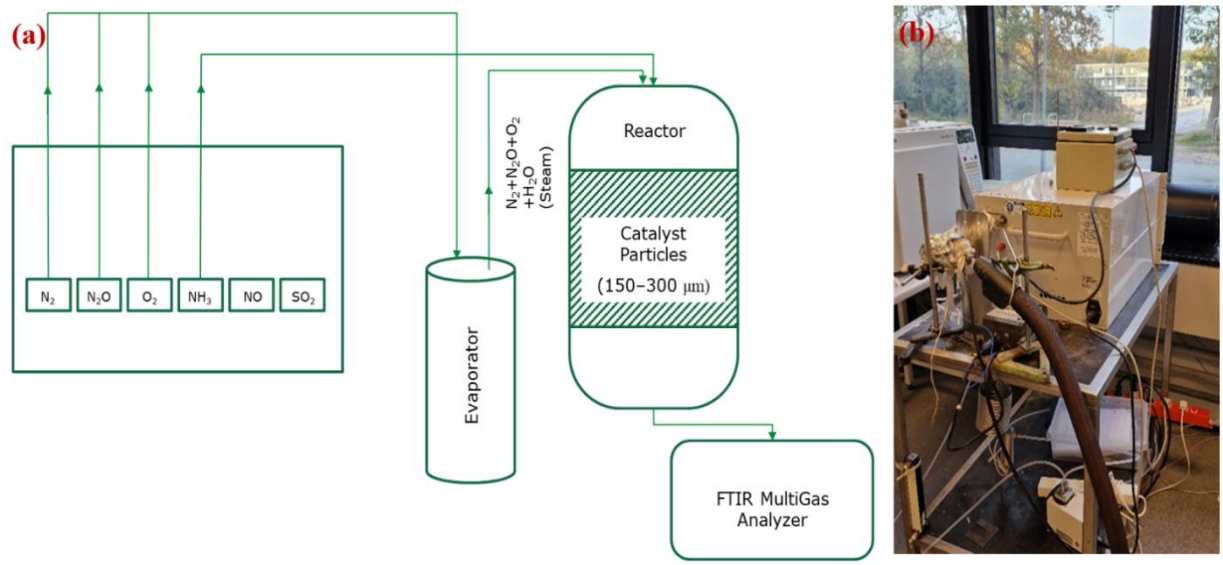

Figure 2. a) Schematic representation of the experimental setup for N_2O removal, and b) On-line gas FTIR for measuring effluent gas composition.

having particles in the size range of 150-300 µm. The composition of the effluent gas stream was measured using an on-line gas FTIR (MKS instruments, Figure 2b) and then discarded into the exhaust vent. The reactor setup has been pictorially and schematically shown in Figure 1 and Figure 2a respectively.

2.1.2 Catalytic testing of Fe-BEA and 0.02K-Co_3O_4 powder catalysts

Following an extensive screening work with different catalytic materials with N_2O abatement potential, we identified Fe-BEA and 0.02K-Co_3O_4 as the most promising candidates.

The Fe-BEA catalyst was procured from Topose and was initially tested for direct decomposition of N_2O in the absence of H_2O. The said catalyst showed good catalytic activity in the temperature range of 400-500°C and achieved an N_2O conversion of ~96% at 500°C. However, as expected, the catalytic activity of the catalyst deteriorated after the introduction of H_2O in the gas stream.

Thereafter, the catalytic activity of the Fe-BEA catalyst was studied with NH_3 present in the feed gas mixture. This is relevant in order to test if the presence of NH_3 is able to accelerate the removal of N_2O, since it is likely that there is unconverted NH_3 coming from the ship engine. Like in the case of direct N_2O decomposition, the catalytic tests for N_2O reduction by NH_3 were carried out both in the presence and absence of H_2O. In the presence of NH_3, the catalytic activity of Fe-BEA improved significantly, and the catalyst achieved full N_2O conversion at 500 °C. In the presence of H_2O and below 450 °C, slightly lower N_2O conversions were recorded than those in the absence of H_2O. However, at 450 °C and beyond, H_2O seemed to have no inhibitory effect on the catalytic activity. Moreover, the overall deterioration in activity due to the presence of H_2O was not as significant as that observed during direct N_2O decomposition.

The 0.02K-Co_3O_4 catalyst was synthesized at DTU via a combination of precipitation and incipient wetness impregnation methods. To synthesize a sample of Co_3O_4, cobalt nitrate hexahydrate ($Co(NO_3)_2.6H_2O$) solution and ammonium bicarbonate ($(NH_4)HCO_3$) solution were added dropwise to a beaker containing deionized water. $(NH_4)HCO_3$ was used as a precipitating agent for this method. The precipitation was carried out at a temperature of 60 °C and a pH of ~9.5. The slurry was stirred for 1 hour and the precipitate was aged for 2 hours. Thereafter, the precipitate was filtered out and washed with deionized water several times and the filter cake was dried at 80 °C overnight. Potassium was then introduced into the precipitate via impregnation and potassium nitrate (KNO_3) was used as the precursor for the same. The nitrate precursor was dissolved in deionized water and the dried precipitate was added to the precursor solution, such that the resulting material has a K/Co molar ratio of 0.02. The amount of water required for preparing the precursor solution was determined by observing the water absorption capacity of a known mass of precipitate. Lastly, the precipitate was dried at 80°C overnight and calcined in air flow at 550 °C for 3 hours.

The 0.02K-Co_3O_4 catalyst was tested for only direct decomposition of N_2O in the presence of H_2O and the said catalyst was found to outperform the Fe-BEA catalyst – even for NH_3-assisted removal of N_2O – over the entire temperature range. The cobalt catalyst achieved an N_2O conversion of ~96% at 400 °C. The light-off curves for the Fe-BEA and 0.02K-Co_3O_4 catalysts under the mentioned conditions are shown in Figure 3.

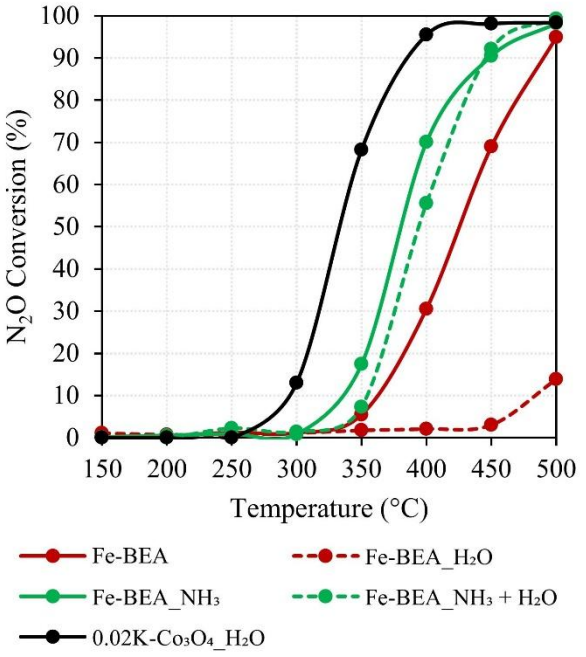

Figure 3. Catalytic activities for direct decomposition and NH_3-assisted removal of N_2O over Fe-BEA catalyst, both in the presence and absence of H_2O and direct decomposition of N_2O over 0.02K-Co_3O_4 catalyst in the presence of H_2O. Reaction conditions: mass of catalyst – 50 mg, gas flow rate – 250 mL/min, N_2O – 250 ppm, NH_3 (if used) – 250 ppm, O_2 – 5%, H_2O (if used) – ~2.5% and N_2 – balance amount.

2.2 Monolith preparation

The preparation of the 0.02K-Co_3O_4 monolith as well as testing and analysis are still on-going, hence in this study the Fe-BEA catalytic monolith is evaluated. The first step of the Fe-BEA monolith preparation is the creation of a slurry for coating onto the monolith. The slurry formulation influences the coating process and as such the rheology of the slurry needs to be carefully evaluated. Additionally, the coating process has also been varied to optimize coating adhesion. Following the coating step is a calcination process and it is after this step where adhesion properties are most critical. Coating adhesion is very important such that

dusting is avoided. This process has been optimized by Topsoe for full monolith preparation as can be seen in Figure 4.

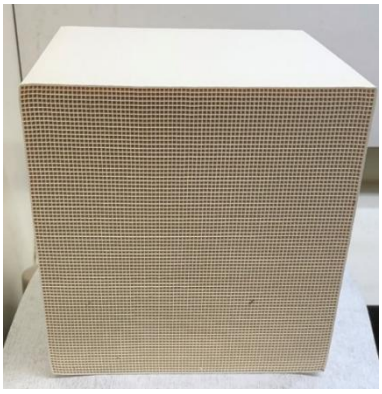

Figure 4. A full-size Fe-BEA monolith with CPSI (cells per square inch) of 400. The Fe BEA is very light in color but gives the monolith a brownish tinge.

2.3 Small-scale catalyst testing

The catalyst chemistry is investigated using the Synthetic Gas Bench (SGB) setup at the Aristotle University of Thessaloniki (AUTH) (Figure 5). Flow rate and gas composition were precisely controlled using programable mass flow controllers (MFCs), while moisture is added to the mixture trough a pre-heated H_2O feed to prevent flue gas condensation. The gas mixture is then heated to the target temperature via a pre-heater system, before passing through the catalyst sample. Outlet species concentrations are measured using an FTIR gas analyser (AVL Seam i60 FT SII).

Two small-scale catalyst samples were tested: a diesel state-of-the-art sample (Pt-AOC) provided by Ecospray and the Fe-BEA monolith prepared by Topsoe. The characteristics of the samples are listed in Table 1.

Table 1. Properties of the tested catalyst samples.

Catalyst sample properties	Fe-SCR	Pt-AOC
Diameter x Length [mm x mm]	28 x 150	28 x 90
Wall thickness [mils]	9	2
Substrate material [-]	cordierite	metal
Cell shape [-]	Square	triangle

The SGB setup allows the realization of steady-state and fully transient tests with sec-by-sec controllable flow rate, temperature and gas compositions. The testing conditions are mentioned in the results section below.

2.4 Mathematical modeling

The mathematical model is based on the solution of the transient heat and species transfer coupled with surface chemistry in the monolith channels based on common literature methods and using the commercial software ExotermiaSuite® [7]. With the assumptions of uniform flow, temperature, and concentration distribution at the monolith face and negligible ambient heat losses, it is sufficient to employ a single channel (1-dimensional) approach.

Temperature and species concentrations along the channel (direction *z*) are determined by solving quasi-steady state balance equations for the heat and mass transfer (Eq.1 and Eq.2):

$$\rho_{\mathrm{g}} C_{\mathrm{p,g}} v_{\mathrm{g}} \frac{\partial T_{\mathrm{g}}}{\partial z} = -h * \left(\frac{S_{\mathrm{F}}}{\varepsilon}\right) * \left(T_{\mathrm{g}} - T_{\mathrm{s}}\right) \quad (1)$$

$$\frac{\partial (v_{\mathrm{g}} y_{\mathrm{g},j})}{\partial z} = -k_j * \left(\frac{S_{\mathrm{F}}}{\varepsilon}\right) * \left(y_{\mathrm{g},j} - y_{\mathrm{s},j}\right) \quad (2)$$

The wall surface temperature is calculated by the transient energy balance of the solid phase expressed as (Eq.3):

$$\rho_{\mathrm{s}} C_{\mathrm{p,s}} \frac{\partial T_{\mathrm{s}}}{\partial t} = \lambda_{s,z} \frac{\partial^2 T_{\mathrm{s}}}{\partial z^2} + S \quad (3)$$

The source term S includes the convective heat transfer (H_{conv}) due to the gas flow in the channels and the heat release (H_{react}) by chemical reactions (Eq.4):

$$S = H_{\mathrm{conv}} + H_{\mathrm{react}} \quad (4)$$

The surface concentrations are obtained by solving the concentration field inside the washcoat layer (direction *w*) via the reaction-diffusion equation (Eq.5):

$$-D_{w,j} \frac{\partial^2 y_{s,j}}{\partial w^2} = \sum_k n_{j,k} R_k \quad (5)$$

The solution of the concentration field in the washcoat layer is of particular importance for the case of technologies with multiple catalytic layers (1D + 1D). In fact, this is the case with ASCs that usually contain two layers, particularly an ammonia oxidation layer at the bottom, as well as an SCR layer on top. This combination comes with advantages concerning NH_3 reduction and selectivity properties of the ASC, as unwanted NO_x formed in the oxidation layer diffuses through the SCR layer where it can be reduced.

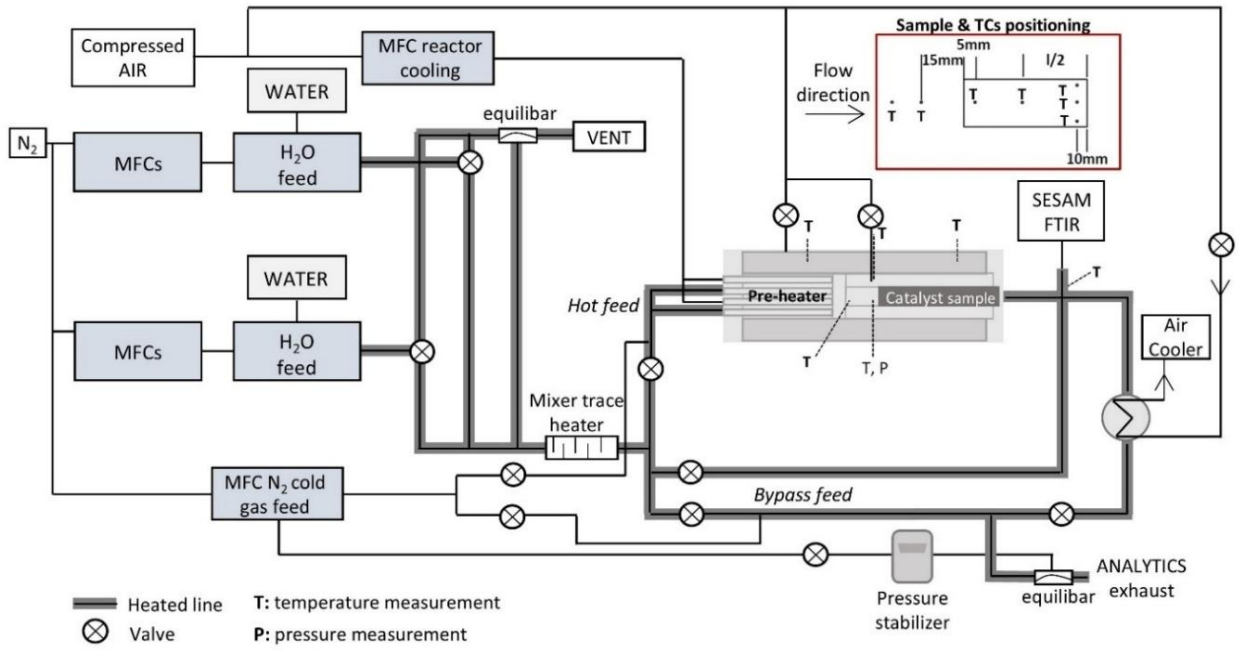

Figure 5. Synthetic Gas Bench (SGB) schematic configuration.

3 RESULTS

3.1 SCR reaction Model for Fe-BEA coating

The SCR reactivity is described adapting commonly used SCR reaction schemes [8], including the standard, fast and NO_2 SCR reactions, as well as NH_3 and NO oxidation, and N_2O formation pathways as listed in Table 2. These reactions, commonly used in Diesel exhaust, served as the starting point. In this section, we are presenting the necessary modifications deemed necessary to describe the SCR chemistry for the Fe-BEA for the NH_3 engine exhaust

Table 2. Basic SCR reaction scheme.

Type	Reaction
NH_3 storage/release	$NH_3 \leftrightarrow NH_3$*
Standard SCR	4 NH_3* + 4 NO + $O_2 \rightarrow$ 4 N_2 + 6 H_2O
Fast SCR	4 NH_3* + 2 NO + 2 $NO_2 \rightarrow$ 4 N_2 + 6 H_2O
NO2 SCR	NH_3 * + 3/4 $NO_2 \rightarrow$ 7/8 N_2 + 3/2 H_2O
N_2O formation pathways	2 NH_3* + 2 NO + $O_2 \rightarrow$ N_2 + N_2O + 3 H_2O 2 NH_3* + 2 $NO_2 \rightarrow$ N_2 + N_2O + 3 H_2O
NO oxidation to NO_2	NO + 1/2 $O_2 \leftrightarrow$ NO_2
NH_3 oxidation	4 NH_3 * + 5 $O_2 \rightarrow$ 4 NO + 5 H_2O 2 NH_3 * + 3/2 $O_2 \rightarrow$ N_2 + 3 H_2O 4 NH_3 * + 4 $O_2 \rightarrow$ 2 N_2O +6 H_2O

Figure 6 shows NO_x and NH_3 conversion vs temperature for ANR=1. According to the standard SCR reaction (4 NO + 4 NH_3 + O_2 → 4 N_2 + 6 H_2O) equal number of moles of NO_x and NH_3 are expected to react. However, test results revealed an overconsumption of NH_3 compared to NO_x. This phenomenon has been documented in several previous studies [9-12]. Consequently, for the model development the stoichiometry of the typical standard SCR reaction was modified as below (Eq.6):

$$6\ NH_3{*} + 5\ NO + 2\ O_2 \rightarrow 11/2\ N_2 + 9\ H_2O \qquad (6)$$

The reaction rate of the modified standard SCR is expressed as (Eq.7):

$$R = k \cdot \Psi_S \cdot \psi_{S_{NH_3}} \cdot C_{NO} \cdot C_{O_2} \qquad (7)$$

The modified standard SCR reaction is able to successfully predict the overconsumption of NH_3 (solid lines of Figure 6).

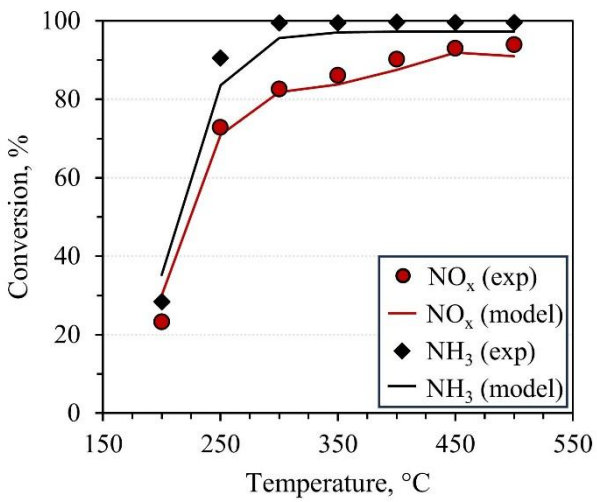

Figure 6. NO_x and NH_3 conversion under Standard SCR conditions based on the experimental data (symbols) and the model (solid lines) (Feed gas: 1000 ppm NO, ANR=1.0, 10% O_2, 15% H_2O, N_2 balance, GHSV=14,000 $^{h-1}$).

The addition of N_2O in the inlet feed gas during deNO_x resulted in an increase of NO_x conversion as shown in (Figure 7).

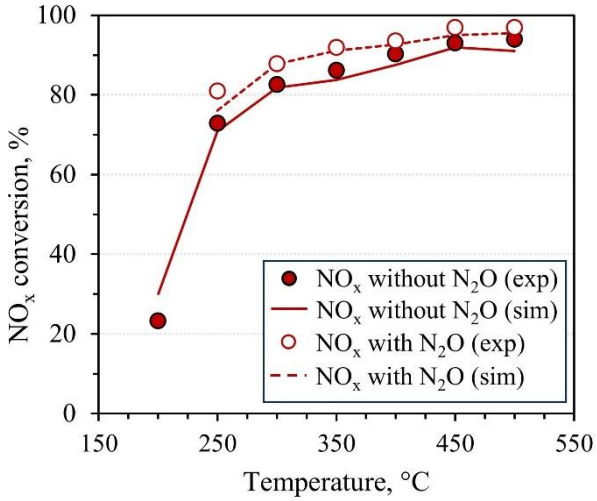

Figure 7. NO_x conversion with and without N_2O over the Fe-SCR based on the experimental data (symbols) and the model (solid lines) (Feed gas: 1000 ppm NO, ANR=1.0, 0 and 100 ppm N_2O, 10% O_2, 15% H_2O, N_2 balance, GHSV=14,000 $^{h-1}$).

To account for this N_2O promotional effect in the model we included a modified reaction with N_2O both in the reactants and products. This suggests that N_2O is not actually consumed but it helps to activate an additional reaction pathway (standard SCR + N_2O, Eq.8):

$$NH_3 + NO + ¼\ O_2 + N_2O \rightarrow N_2 + 3/2\ H_2O + N_2O \quad (8)$$

The addition of this reaction results in satisfactory accuracy of the model and the experimental data.

The conversion of N_2O over the Fe-BEA catalyst in the presence and absence of NH_3 could be adequately reproduced by the model using the following reaction scheme [13,14]:

$$2\ NH_3 + 3\ N_2O \rightarrow 4\ N_2 + 3\ H_2O \quad (9)$$

$$NH_3 + NO + N_2O + ¼\ O_2 \rightarrow N_2 + 3/2\ H_2O + N_2O \quad (10)$$

The final Fe-BEA reaction scheme is summarized in Table 3.

Table 3. Fe-BEA reaction scheme.

Type	Reaction
NH_3 storage/release	$NH_3 \leftrightarrow NH_3$*
Modified Standard SCR	6 NH_3* + 5 NO + 2 $O_2 \rightarrow$ 11/2 N_2 + 9 H_2O
Standard SCR (+N_2O)	NH_3* + NO + 1/4 O_2 + $N_2O \rightarrow N_2$ + 3/2 H_2O +N_2O
Fast SCR	NH_3* + ½ NO + ½ $NO_2 \rightarrow N_2$ + 3/2 H_2O
N_2O formation pathways	2 NH_3* + 2 NO + $O_2 \rightarrow N_2$ + N_2O + 3 H_2O 2 NH_3* + 2 $NO_2 \rightarrow N_2$ + N_2O + 3 H_2O
NO oxidation to NO_2	NO + 1/2 $O_2 \leftrightarrow NO_2$
NH_3 oxidation to N_2	NH_3* + 3/4 $O_2 \rightarrow$ ½ N_2 + 3/2 H_2O
N_2O reduction by NH_3	2 NH_3* + 3 $N_2O \rightarrow$ 4 N_2 + 3 H_2O
Simultaneous reduction of NO and N_2O by NH_3	2 NH_3* + 2 NO + $N_2O \rightarrow$ 3 N_2 + 3 H_2O

Figure 8 summarizes the model performance for NO_x, NH_3 and N_2O prediction in a wide range of temperatures and ANR.

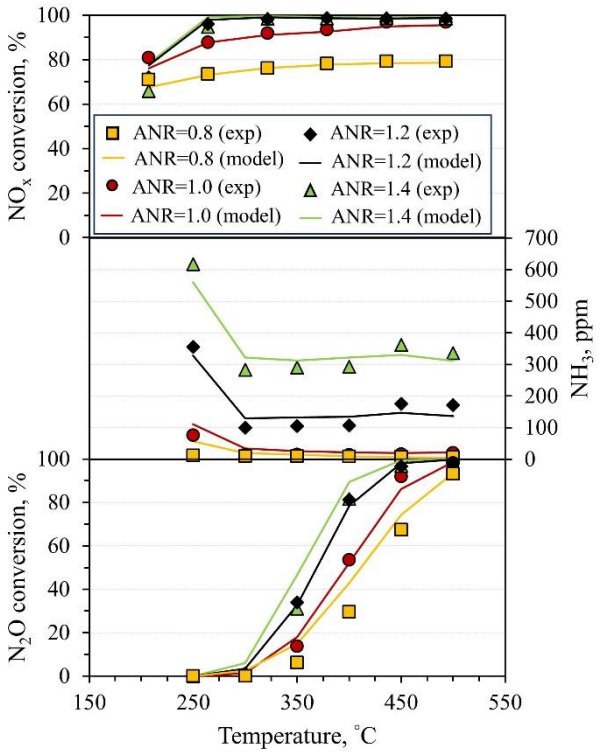

Figure 8. NO_x conversion, NH_3 slip and N_2O conversion over the Fe-BEA based on the experimental data (symbols) and the model (solid lines) (Feed gas: 1000 ppm NO, ANR=0.8*, 1.0, 1.2, 1.4, N_2O=100, 200*, 10% O_2, 15% H_2O, N_2 balance, GHSV=20,000 $^{h-1}$).

For ANR less than 1, the NO_x conversion is limited by the lack of NH_3 as expected. The targeted 80% NO_x conversion is achieved at temperatures above 250°C while N_2O conversion above 80% takes place at higher temperatures above 400°C.

3.2 Reaction Model for the Pt-based coating

Ammonia oxidation on the Pt-AOC catalyst is modeled using a common kinetic approach, which effectively describes the overall reactions [15]. The reactions used are listed in and include the oxidation of NH_3 to N_2 and NO, the simultaneous oxidation of NH_3 and NO to N_2O and the bi-directional oxidation of NO to NO_2.

Table 4. Basic Pt-AOC reaction scheme.

Type	Reaction
NO oxidation to NO_2	$NO + 1/2\ O_2 \leftrightarrow NO_2$
NH_3 and NO oxidation to N_2O	$2\ NH_3 + 2\ NO + 3/2\ O_2 \rightarrow 2\ N_2O + 3\ H_2O$
NH_3 oxidation	$4\ NH_3 + 5\ O_2 \rightarrow 4\ NO + 5\ H_2O$ $2\ NH_3 + 3/2\ O_2 \rightarrow N_2 + 3\ H_2O$

The experimental and respective model are depicted in Figure 9.

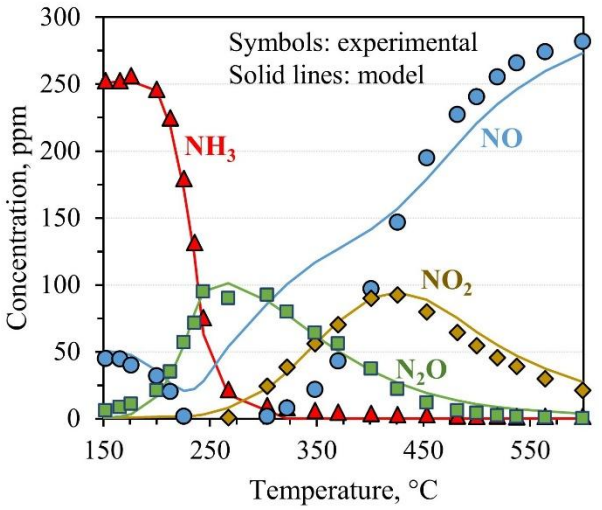

Figure 9. Comparison of the NH_3, NO, NO_2 and N_2O outlet concentrations for NH_3 oxidation over the Pt-AOC based on the experimental data (symbols) and the model (solid lines) (Feed gas: 250 ppm NH_3, 50 ppm NO, 6% O_2, 15% H_2O, 15 ppm SO_2, N_2 balance, GHSV=20,000 $^{h-1}$).

The analysis focuses not only on NH_3 reduction but also on the formation of undesired byproducts, including NO_x and N_2O. The NH_3 concentration decreases sharply between 200°C and 250°C, achieving complete oxidation around 300°C. N_2O formation is evident above 200°C, reaching a peak concentration of 100 ppm at 250°C. Above that temperature, formation of NO and NO_2 becomes predominant while N_2O decreases. Notably, the calibrated model accurately predicts the complex trends of N_2O and NO_x byproduct formation across the entire temperature range.

3.3 Sulfur tolerance of the Fe-BEA coating

The Fe-BEA is initially exposed to 110 ppm SO_2 at 225°C until saturation (approximately 25 minutes) as presented in Figure 10a. The maximum SO_2 stored on the catalytic sites is calculated equal to 1.13 g/l. Subsequently, an SCR experiment is conducted without further exposure to sulfur, as presented in Figure 10b. Compared to the fresh catalyst, a reduction in NO_x conversion is observed at temperatures below 300°C, whereas NO_x conversion efficiency remained unaffected by sulfur at higher temperatures. Regarding N_2O formation, the saturated catalyst exhibited similar activity to the fresh catalyst (Figure 10c).

High temperature desulfation is then investigated (Figure 10d). The catalyst is exposed to temperatures above 400°C for 30 minutes, followed by NO_x conversion measurements at 250°C, where reduced NO_x conversion is initially observed. Partial recovery of catalytic efficiency was achieved

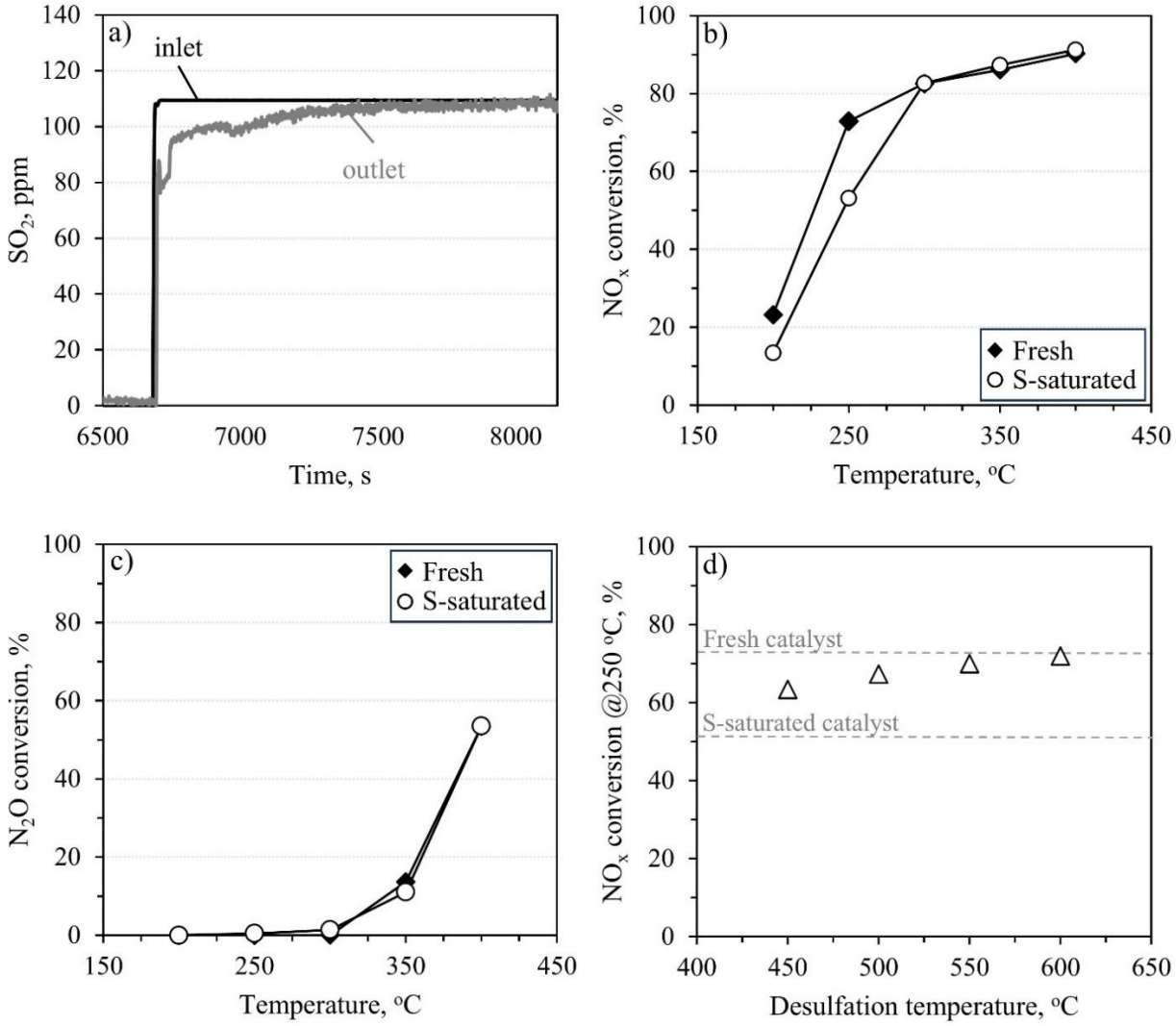

Figure 10. (a) Exposure of the Fe-BEA catalyst to SO_2, (b) NO_x conversion of the fresh and s-saturated catalyst, (c) N_2O conversion of the fresh and s-saturated catalyst, (d) desulfation of the catalyst at high temperatures. (Feed gas (a) 1000 ppm NO, ANR=1.0, 15% H_2O, 10% O_2, N_2 balance, GHSV=14,000h-1; Feed gas (b), (c), (d): 1000 ppm NO, ANR=1.0, 100 ppm N_2O, 15% H_2O, 10% O_2, N_2 balance, GHSV=14,000h-1).

at a desulfation temperature of 450°C, and full activity restoration is observed at 600°C.

3.4 Model Application in Marine Engine Exhaust

3.4.1 Boundary conditions

In this section we will use the EATS model with boundary conditions corresponding to the expected exhaust gas conditions of an NH_3 engine. The target is to determine the architecture, the dimensions and the dosing control that achieve the best compromise in terms of harmful pollutants and greenhouse gas emissions reduction.

Given that NH_3 engines are still under development and not yet commercially available, precise data on exhaust gas conditions (temperature and chemical composition) are not well known. This is not unexpected, since the exhaust gas composition in terms of NO_x, N_2O and NH_3 strongly depend on the local temperature and stoichiometry in the cylinder. Therefore, these emissions are highly sensitive to the spray mixing and combustion processes that can be adjusted to a certain extent via injection related geometrical parameters and timing. From the initial results of the ENGIMMONIA project, we already have some estimates regarding expected engine out conditions as function of engine load that can be used as boundary conditions for the model-based analysis (Table 5). These values

correspond to an engine with rated max power around 6.2 MW at 123 rpm.

As shown in this table, the exhaust gas temperature at pre-turbo position is marginally within the range of high catalytic activity for the SCR reactions and unfortunately lower than the temperature required for efficient N_2O reduction. Therefore, the positioning of the EATS behind the turbine where the temperature is much lower has been excluded at this phase.

It can be noted that the exhaust gas temperature is expected to be lower compared to the respective one expected with Diesel-only mode possibly due to the lower NH_3 adiabatic flame temperature [16,17].

Table 5. Engine out (pre-turbo) expectations from ENGIMMONIA project data for NH_3 operation.

Engine Load, %	25	50	75	100
Exhaust gas temperature, °C	285	285	305	355
Exhaust gas pressure, bar	1.4	2.0	3.0	3.9
Exhaust gas mass flow, kg/s	4	9	12	15
CO_2 from pilot fuel, %	1	0.9	0.7	0.6
NO_x, ppm	500 - 1000			
NH_3, ppm	500 - 1000			
N_2O, ppm	5 - 20			

According to the initial test results, NO_x and NH_3 emissions are expected to lie in the range between 500 – 1000 ppm whereas N_2O is expected to be close to 10 ppm. However, for the sake of completeness and due to the high relevance of N_2O emissions on the GHG reduction potential, we will consider cases of 5 ppm and 20 ppm N_2O concentrations.

The GHG emissions will be evaluated accounting for both N_2O (originating from NH_3 combustion and the EATS), and CO_2 from pilot-fuel combustion. The total GHG emissions at each operating point (load) are calculated as (Eq.11):

$$\text{Total GHG} = N_2O \text{ x } 265 + CO_2 \text{ from pilot fuel} \qquad (11)$$

The weighted average GHG emissions reduction compared to Diesel-only operation is calculated based on the weighting factors of the legislated E3 test cycle [18].

3.4.2 Simulation cases

As mentioned above, the engine can be designed and/or calibrated for different ANR, therefore we will report three potential cases, each one with different exhaust layout requirements as summarized in Table 6:

Table 6. Case descriptions.

Case	NO_x	NH_3	N_2O	ANR	Layout
1a	1000	500	5	0.5	SCR+NH_3 injection
1b	1000	500	20	0.5	SCR+NH3 injection
2a	1000	1000	5	1.0	SCR no injection
2b	1000	1000	20	1.0	SCR no injection
3a	900	1000	5	1.1	SCR+ASC
3b	900	1000	20	1.1	SCR+ASC

All the simulations aim at achieving safe NO_x emissions compliance with Tier III regulated limit of 3.4 g/kWh without exceeding 10 ppm of NH_3 slip. The achievement of this target usually requires an iterative process of optimizing both catalyst volumes and NH_3 dosing when applicable. In order to limit the complexity and optimization dimensions for the purpose of the paper, we assume fixed geometries and catalyst configurations for all 3 cases (Table 6). It can be noted that the ASC catalyst is composed of a bottom PGM and a top SCR layer. These properties have been obtained as reasonable compromises between efficiency/costs from previous work. Nevertheless, this analysis can be readily expanded to include catalyst optimizations on a per case basis.

Table 7. Properties of the modelled EATS.

Technology	Volume, l	Washcoat loading, g/l	PGM loading, g/ft^3	CPSI, -
Fe-BEA	1135	240	-	85
ASC (SCR layer)	430	70	-	85
ASC (PGM layer)		60	15	85

In Case 1, NH_3 injection upstream of the SCR is required as shown in Figure 11 (Case 1) to achieve the target NO_x limit of 3.4 g/kWh. Based on the weighting factors of the legislated E3 test cycle [18], it is estimated that a NO_x conversion rate in the order of 75% is required to comply with the Tier III limit of 3.4 gNO_x/kWh. To achieve this, it is necessary to inject additional NH_3 up to a ratio of ANR equal to around 0.8 upstream of the SCR.

In Case 2 an SCR-only configuration is used without any NH_3 injection and ANR equal to 1. (Figure 11, Case 2).

In Case 3, a dual-layer ASC is placed downstream of the SCR to treat the unreacted NH_3 of the deNO_x process (Figure 11, Case 3). Based on simulation analysis, we found that ANR>1.1 would result in excessively high N_2O, therefore we use here an ANR=1.1. Further analysis on the effect of ANR on N_2O formation in the case of excess NH_3 is

presented in the next section (3.4.3). The ASC is assumed to be a combination of an Fe-BEA SCR layer and a precious metal-based layer (Pt-AOC). The chemical composition of the SCR layer is identical to the SCR catalyst prior to the ASC.

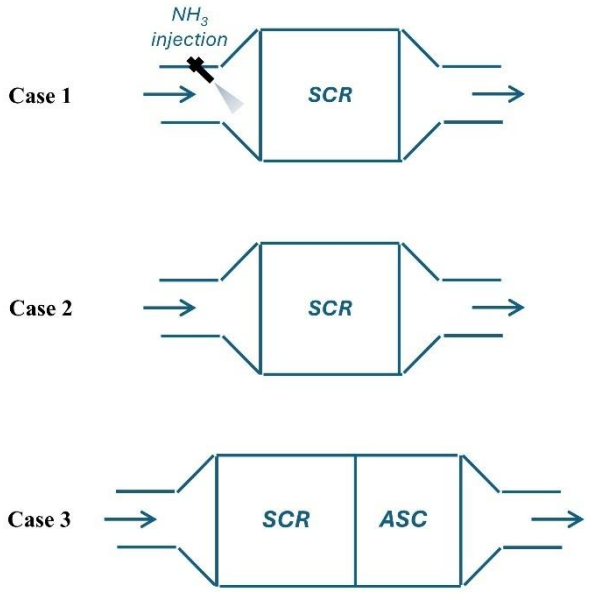

Figure 11. Model exhaust layouts for the examined 3 cases: Case 1 minimum ANR<1, Case 2 maximum ANR (SCR no injection), and Case 3 ANR>1 (SCR+ASC).

Applying the simulation model to the four loads of the E3 test cycle [18] under the conditions specified in Table 5 and the exhaust gas concentrations specified in Table 6 , NO_x, NH_3 slip GHG from N_2O as well as total GHG emissions are calculated at the system outlet as presented in Figure 12 and Figure 13.

The weighted average NO_x emissions are consistently maintained below the Tier III regulatory limits across all configurations (Figure 12). Significantly lower NO_x levels are expected in the SCR-only and SCR+ASC systems, attributed to the abundant availability of NH_3 to react with NO_x.

Figure 13 shows the calculated NH_3 slip levels, which are kept below 10 ppm thanks to the optimization of catalyst volumes and NH_3 dosing where applicable. N_2O emissions expressed in GHG equivalent are quite higher at low loads due to the low temperature. In the case of excessive NH_3 in the exhaust gas (SCR+ASC), N_2O is observed to be higher compared to the other cases due to the high formation of N_2O during NH_3 oxidation within the ASC even at low levels of excessive NH_3. A substantial decrease of N_2O is observed only at 100% engine load thanks to the sufficient exhaust gas temperature.

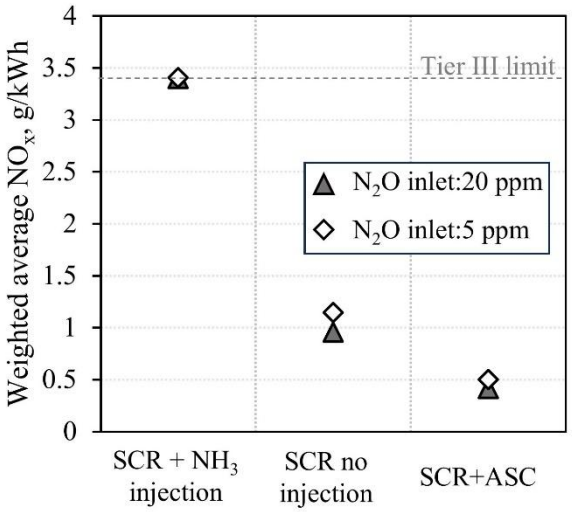

Figure 12. Weighted average NO_x emissions for the three examined cases of NH_3 operation.

To evaluate the suitability of the NH_3-optimized exhaust systems configurations, these are applied in 100% Diesel exhaust using the engine-out conditions of Table 8. Since Diesel combustion does not produce any NH_3, the latter needs to be injected prior to the SCR in all cases, hence Case 1 (SCR+NH_3 injection) and Case 3 (SCR+ASC) with NH_3 injection are applied.

Table 8. Engine out (pre-turbo) expectations Diesel operation.

Engine Load, %	25	50	75	100
Exhaust gas temperature, °C	305	335	370	450
Exhaust gas pressure, bar	1.4	2.1	3.1	4.0
Exhaust gas mass flow, kg/s	4	9	12	15
CO_2, g/kWh	534	510	518	540
NO_x, ppm	2500	2200	1800	1600

The NH_3 injection rate is tuned in both cases to achieve Tier III NO_x limit. NH_3 slip, N_2O and total GHG emissions are calculated at the system outlet as depicted in Figure 14. Almost all injected NH_3 is consumed during NO_x reduction, while N_2O production in the EATS is below 5ppm. The total GHG emissions (CO_2 from combustion + N_2O produced in the EATS) are higher than 500 g/kWh at all operating conditions.

In terms of NO_x and NH_3 emissions, the NH_3-optimized exhaust gas configurations work efficiently in Diesel operation.

Figure 15 illustrates the average GHG emissions reduction for the three cases of NH_3 operation compared to 100% Diesel-only operation. The results indicate that all configurations achieve 75-

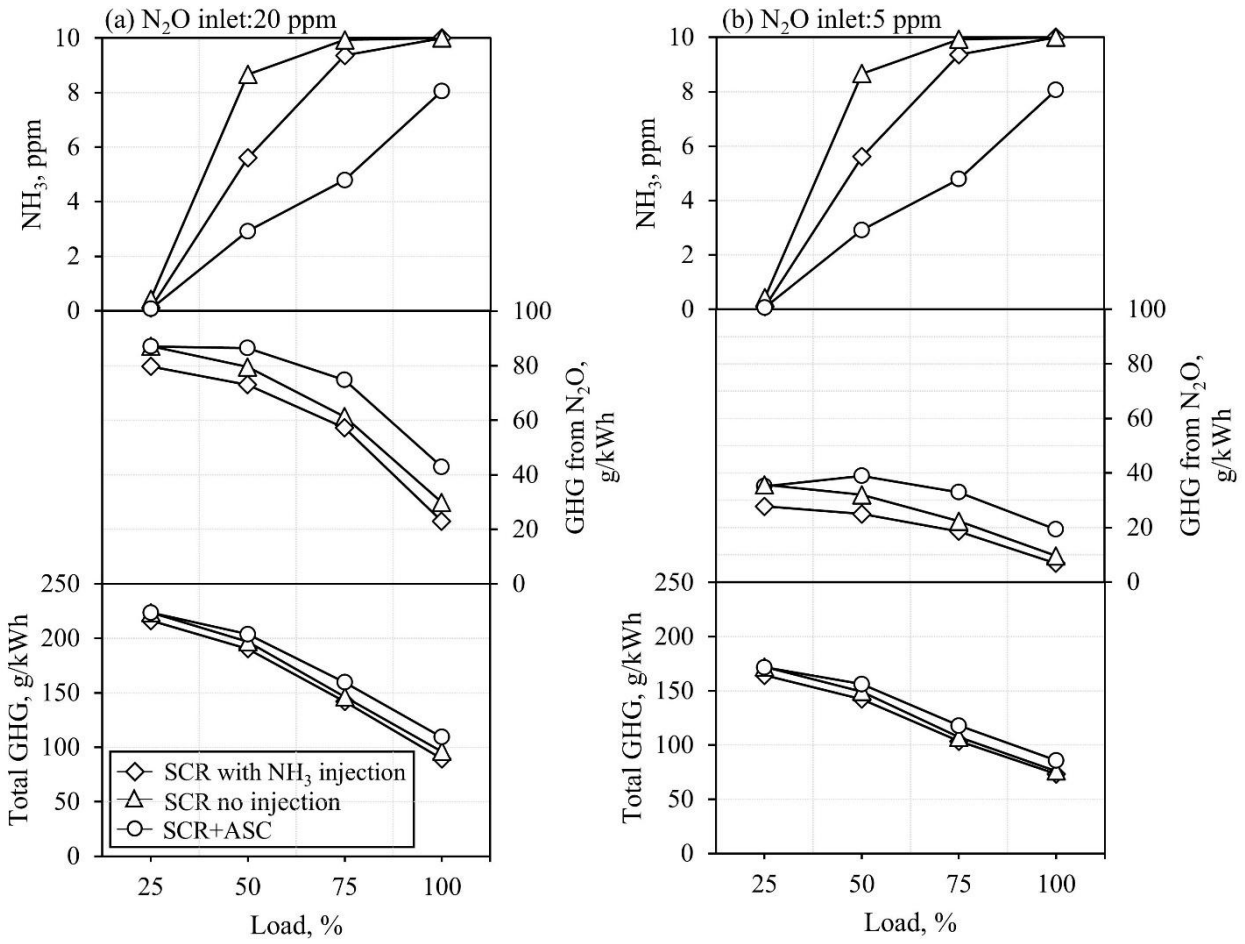

Figure 13. NH_3 slip, GHG emission from N_2O and total GHG emissions (N_2O+CO_2 from pilot fuel) at the EATS outlet for the three tested cases with (a) 20 ppm N_2O, and (b) 5 ppm N_2O in the NH_3 exhaust gas.

80% reduction provided that engine-out N_2O is 5 ppm, which drops to 65-70% when this concentration increases to 20 ppm. These findings indicate the critical role of N_2O control in optimizing GHG emissions reduction.

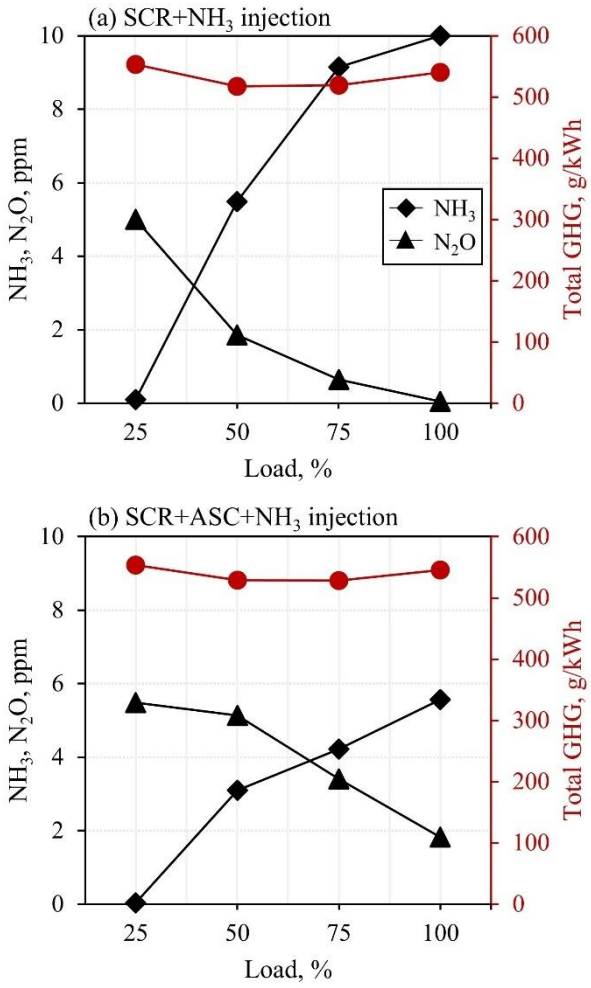

Figure 14. NH_3, N_2O and total GHG emissions of Diesel operation in (a) Case 1 (SCR+NH_3 injection) and (b) Case 3 (SCR+ASC+NH_3 injection).

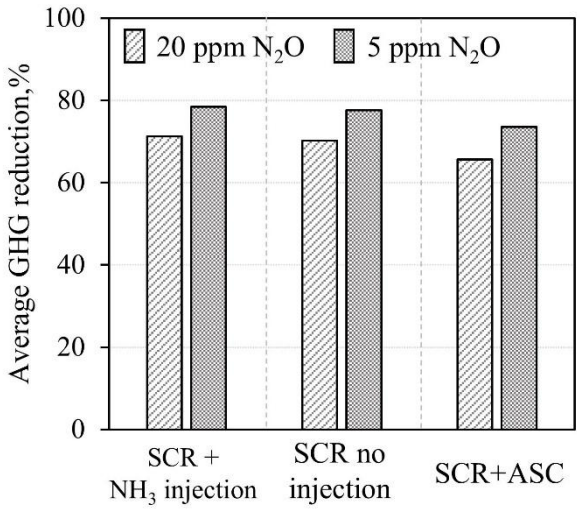

Figure 15. GHG emissions reduction percentage compared to 100% Diesel operation under the E3 cycle, for the three examined cases with 5 ppm and 20 ppm N_2O in the exhaust gas.

3.4.3 Effect of NH_3 combustion efficiency

The incomplete NH_3 combustion unavoidably leads to NH_3 engine-out emissions which have to be treated catalytically. In the previous section, we examined the case of NH_3=1000 ppm which corresponds to a combustion efficiency equal to ~88% at 25% up to ~ 94% at full load. The NO_x emissions in Case 3 (SCR+ASC) were assumed equal to 900 ppm, so ANR was ~1.1. Here we examine the impact of combustion efficiency on the resulting NH_3 engine-out and catalyst-out emissions as well as the resulting N_2O and the respective GHG impact. The NO_x emissions at the engine-out are assumed to be constant while unburnt NH_3 is varied according to the combustion efficiency using stoichiometric calculations accounting also for the contribution of pilot Diesel. The EATS is optimized at each ANR to achieve NH_3 slip below 10 ppm while NO_x emissions comply with Tier III limit.

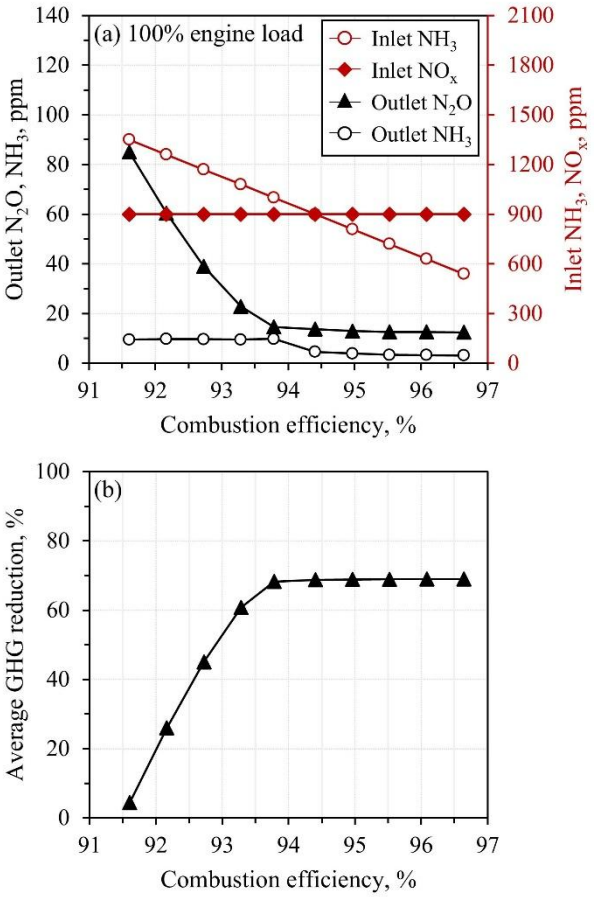

Figure 16. (a) N_2O at the SCR+ASC system outlet and NH_3 and NO_x at system inlet at 100% load, and (b) average GHG emissions reduction percentage compared to Diesel operation based on the weighting factors of the E3 test cycle [19], under various ANR. Optimized system to achieve NO_x below Tier III limit and NH_3 slip below 10 ppm (Inlet

feed gas: 900 ppm NO, variable NH_3, 20 ppm N_2O, N_2 balance).

When the combustion efficiency is low, engine-out NH_3 emissions are higher which eventually leads to increased N_2O formation in the EATS as illustrated in Figure 16a. Please, note that these results refer to the 100% engine load only. As a result, the reduction in GHG emissions diminishes, approaching the levels of Diesel operation when the combustion efficiency goes below 91.5% which corresponds to 1350 ppm inlet NH_3 (ANR=1.5) (Figure 16b).

Consequently, when the combustion efficiency is higher than ~ 94% (at 100% load), a reasonable level of GHG reduction of the order of 70% is achievable without additional deN_2O measures. The percentage is higher if engine out N_2O emissions are kept further below 20 ppm. Research is going on with catalytic formulations that could decompose N_2O in the unfavorable low-temperature marine exhaust gas. Co-based catalysts have been studied with initially promising results, however without yet solving the low-temperature efficiency [19,20].

4 CONCLUSIONS AND FUTURE WORK

This study demonstrates the potential of NH3-fueled 2-stroke engines to reduce GHG emissions in marine applications.

It is shown that the conventional SCR-only system using an Fe-BEA catalyst can meet the emissions target and achieve GHG reduction of the order of 70% only if the ANR upstream the SCR is kept close to 0.8-1.

For cases with ANR>1 which is relevant for combustion efficiencies lower than ~95%, the implementation of an ASC in the EATS is necessary to control the excess NH_3 emissions. Due to the side reactions in the ASC, this comes with a significant N_2O formation, thereby reducing the GHG reduction potential. A minimum combustion efficiency of approximately 94% at 100% engine load is required to achieve a 70% GHG reduction compared to Diesel operation. Below this threshold, there is a need for additional deN_2O measures to justify the GHG benefits of NH_3 combustion.

Ongoing research focuses on the development and evaluation of catalytic formulations capable of decomposing N_2O under the challenging low-temperature conditions of marine exhaust gases. Cobalt-based catalysts have shown initially promising results, however, achieving efficient N2O decomposition at low temperatures remains unresolved. Current and future work includes extensive testing and modeling of these catalysts to improve their performance and suitability for marine engine applications.

5 DEFINITIONS, ACRONYMS, ABBREVIATIONS

A. Latin letters

C: Species molar concentration mol/m^3

C_p: Specific heat capacity $J/(kg \cdot K)$

D_w: Effective diffusivity m^2/s

h: Heat transfer coefficient $W/(m^2 \cdot K)$

k: Arrhenius term -

k_j: Mass transfer coefficient m/s

n: Stoichiometric coefficient –

R_k: Reaction rate $mol/(m^3 \cdot s)$

S: Heat source term W/m^3

S_F: Monolith specific surface area m^2/m^3

T: Temperature K

v: Velocity m/s

w: Dimension perpendicular to wall surface -

y_j: Molar fraction -

z: Axial coordinate along monolith m

B. Greek Letters

ε: Macroscopic void fraction -

λ: Thermal conductivity $W/(m \cdot K)$

ρ: Density kg/m^3

Ψ_S: Storage capacity of storage site

$\psi_{S_{NH_3}}$: Surface coverage fraction of NH_3

C. Subscripts and Superscripts

g: Exhaust gas

j: Species Index

k: Reaction Index

s: Solid

6 FUNDING

This work has been performed in the framework of the ENGIMMONIA project, which has received funding from the European Union's Horizon 2020 research and innovation program under grant agreement Nr. 955413.

7 ACKNOWLEDGMENTS

The authors would like to acknowledge support of this work by Ecospray for providing the Pt-based catalyst and TOPSOE for providing the Fe-based catalysts and useful discussions during the experimental campaign.

8 REFERENCES AND BIBLIOGRAPHY

[1] International Maritime Organization. Fourth IMO GHG Study Full Report. 2020. London, UK.

[2] Liu, L., Wu, J., Liu, H., Wu, Y., Wang, Y. 2024. Investigation of combustion and emission characteristics in a low-speed marine engine using ammonia under thermal and reactive atmospheres. *Int. J. Hydrogen Energy*, 1237-1247.

[3] IMO Marine Environment Protection Committee. Eightieth Session (MEPC 80)-Summary Report; International Maritime Organization: London, UK, 2023.

[4] DNV GL AS Maritime. 2019. Comparison of Alternative Marine Fuels Report. Norway.

[5] Rodríguez, C.G., Lamas, M.I., Rodríguez, J.d.D., Abbas, A. 2022. Possibilities of Ammonia as Both Fuel and NO_x Reductant in Marine Engines: A Numerical Study. *J. Mar. Sci. Eng.*, 10, 43.

[6] Wang, Q., Yang, W., Dang, H., Li, L., Wu, R., Wang, Y., Zhao, Y. 2024. Enhancement of N_2O Decomposition Performance by co-doping of Ni and Y to Co_3O_4 catalyst. *J. Environmental Chemical Engineering*, 12, 112463.

[7] Exothermia, S.A. 2022. Exothermia Suite User Manual, version 2022.3; Gamma Technologies, LLC: Westmont, IL, USA.

[8] Karamitros, D., Koltsakis, G. 2017. Model-based optimization of catalyst zoning on SCR-coated particulate filters. *Chem. Eng. Sci.*, 173, 514-524.

[9] Sjövall, H., Blint, R. J., Gopinath, A., Olsson, L. 2010. A Kinetic Model for the Selective Catalytic Reduction of NO_x and NH_3 over an Fe-zeolite Catalyst. *Ind. Eng. Chem. Res.*, 49, 39-52.

[10] Nedyalkova, R., Kamasamudram, K., Currier, N. W., Li, J., Yezerets, A. 2013. Experimental evidence of the mechanism behind NH_3 overconsumption during SCR over Fe-zeolites. *Journal of Catalysis*, 299, 101-108.

[11] Bacher, V., Perbandt, C., Schwefer, M., Siefert, R., Pinnow, D., Turek, T. 2015. Kinetics of ammonia consumption during the selective catalytic reduction of NO_x over an iron zeolite catalyst. *Applied Catalysis B: Environmental*, 162, 158-166.

[12] Liu, Q., Bian, C., Ming, S., Guo, L., Zhang, S., Pang, L., Liu, P., Chen, Z., Li, T. 2020. The opportunities and challenges of iron-zeolite as NH_3-SCR catalyst in purification of vehicle exhaust. *Applied Catalysis A*, 607, 117865.

[13] Zhang, X., Shen, Q., He, C., Ma, C., Chen, J., Li, L., Hao, Z. 2012. Investigation of Selective Catalytic Reduction of N_2O by NH_3 over an Fe-Mordenite Catalyst: Mechanism and O_2 Effect. *ASC Catal*., 2, 512-520.

[14] Coq, B., Mauvezin, M., Delahay, G., Butet, J. B., Kieger, Stephane. 2000. The simultaneous catalytic reduction of NO and N_2O by NH_3 using an Fe-zeolte-beta catalyst. *Applied Catalysis B: Environmental,* 27, 193-198.

[15] Colomb, M., Nova, I., Tronconi, E., Schmeißer, V., Brandl-Konrad, B. Zimmermann, L.R. 2013. Experimental Modeling Study of a dual-layer (SCR + PGM) NH_3 slip monolith catalyst (ASC) for automotive SCR aftertreatment systems. Part I. Kinetics for the PGM Component and Analysis of SCR/PGM Interactions. *Appl. Catal. B Environ*., 142–143, 861–876.

[16] Zhu, Y., Xia, C., Shreka, M., Wang, Z., Yuan, L., Zhou, S., Feng, Y., Hou, Q., Ahmed, S.A. 2020. Combustion and emission characteristics for a marine low-speed diesel engine with high-pressure SCR system. *Environ. Sci. Pollut. Res*., 27, 12851–12865.

[17] Zhu, Y., Li, T., Xia, C., Feng, Y., Zhou, S. 2020. Simulation analysis on vaporizer/mixer performance of the high-pressure SCR system in a marine diesel. *Chem. Eng. Process.-Process Intensif.*, 148, 107819.

[18] MARPOL, Annex VI—Regulations for the Prevention of Air Pollution from Ships, Appendix II—Test Cycles and Weighting Factors (Regulation 13). Available online: http://www.marpoltraining.com/MMSKOREAN/MARPOL/Annex_VI/app2.htm

[19] Xue, L., Zhang, C., He, H., Teraoka, Y. 2007. Catalytic decomposition of N_2O over CeO_2 promoted Co_3O_4 spinel catalyst. *Applied Catalysis B: Environmental*, 75, 167-174.

[20] Kim, M. J., Lee, S. J., Ryu, I. S., Jeon, M. W., Moon, S. H., Roh, H. S., Jeon, S. G. 2017. Catalytic decomposition of N_2O over cobalt based spinel oxides: The role of additives. *Molecular Catalysis*, 442, 202-207.